The Journal of Experimental Biology 214, 521-529

doi:10.1242/jeb.050567

RESEARCH ARTICLE

The mechanics of explosive dispersal and self-burial in the seeds of the filaree, *Erodium cicutarium* (Geraniaceae)

Dennis Evangelista[1,*], Scott Hotton[2] and Jacques Dumais[2]

[1]Department of Integrative Biology, University of California, Berkeley, Berkeley, CA 94720, USA and [2]Department of Organismic and Evolutionary Biology, Harvard University, Cambridge, MA 02138, USA

*Author for correspondence (devangel@berkeley.edu)

Accepted 8 November 2010

SUMMARY

The filaree (*Erodium cicutarium*), a small, flowering plant related to geraniums, possesses a unique seed dispersal mechanism: the plant can fling its seeds up to half a meter away; and the seeds can bury themselves by drilling into the ground, twisting and untwisting in response to changes in humidity. These feats are accomplished using awns, helical bristles of dead but hygroscopically active tissue attached to the seeds. Here, we describe the kinematics of explosive dispersal and self-burial based on detailed high-speed and time-lapse videos. We use these observations to develop a simple mechanical model that accounts for the coiling behavior of the awn and allows comparison of the strain energy stored in the awn with the kinetic energy at launch. The model is used to examine tradeoffs between dispersal distance and reliability of the dispersal mechanism. The mechanical model may help in understanding the invasive potential of this species and provides a framework for examining other evolutionary tradeoffs in seed dispersal mechanisms among the Geraniaceae.

Supplementary material available online at http://jeb.biologists.org/cgi/content/full/214/4/521/DC1

Key words: *Erodium cicutarium*, seed dispersal, awn, bending, hygroscopic movement, burial, biomechanics, fast movement in plants, ballistic movement.

INTRODUCTION

The ability of seeds to disperse away from the parent plant and bury themselves can improve their chances of germinating and surviving. Explosive dispersal and self-burial can be accomplished using awns, hair-like appendages that launch seeds by storing elastic energy and subsequently move them across or into the soil using hygroscopically powered shape changes. Examples of this dispersal mechanism have been described in black oat grass (*Stipa avenacea*), wiregrass (*Aristida tuberculosa*), wheat (*Triticum* sp.), mouse barley (*Hordeum murinum*) and the musky heron's bill (*Erodium moschatum*) (Murbach, 1900; Collins and Wein, 1997; Elbaum et al., 2007; Wolgemuth, 2009; Stamp, 1989a). Members of the genus *Erodium* are widely distributed and invasive in several USA states, which some have attributed to their ability to disperse actively and bury themselves (Mensing and Byrne, 1998). Self-burial appears to enhance seedling survivorship (Stamp, 1989a), whereas dispersal ability is correlated with the spacing and size of patches and environmental heterogeneity at several scales (Stamp and Lucas, 1983; Stamp, 1989b; Baythavong et al., 2009).

Erodium cicutarium (Fig. 1) is a spring-flowering annual with small, pink flowers with five petals. After flowering, the fruits, which consist of five mericarps joined together, grow a large spine-like style. The style consists of the awns of each mericarp joined together. As the fruits dry, stresses develop within the awns, causing them to separate abruptly and flinging the seeds some distance away from the parent plant (explosive dispersal) (Stamp, 1989a). The preferred shape of dry awns is helical, but while in the fruit they are held straight by being joined together in the style.

Once on the ground, humidity changes cause the awns to unwind straight when wet, or rewind back to their helical shape when dry. The resulting motor action, combined with hairs on the seed and along the length of the awn, moves the seeds across the surface, eventually lodging them into a crevice and causing them to drill themselves into the ground (self-burial) (Stamp, 1984).

A mechanical model capable of describing the explosive release and self-burial of *Erodium* seeds would allow exploration of potential tradeoffs in this intriguing dispersal mechanism, and could be used to test hypotheses about the evolution of dispersal in the Geraniaceae. With this goal in mind, we developed a beam-bending model that accounts for the helical shape changes of the awn during burial, and used it to compute energy storage before launch. Using standard equations from fracture mechanics and ballistics, we estimated the energy released on launch and predicted the dispersal range and seed trajectory. These predictions were compared with measured kinematics and dispersal distances from high-speed filming of awn launches. Finally, we used the model to explore two fundamental tradeoffs in the *Erodium*-type dispersal mechanism.

Two important tradeoffs

Fracture at minimum energetic cost is needed to maximize dispersal distance. However, a premature fracture risks launching the seed before it has stored sufficient energy to reach appreciable range, resulting in a short range 'dud'. The two-sided constraint, in which the work of fracture must be high enough to prevent premature fracture but low enough to maximize ejection distance, is in sharp contrast to classical fracture mechanics problems where avoidance

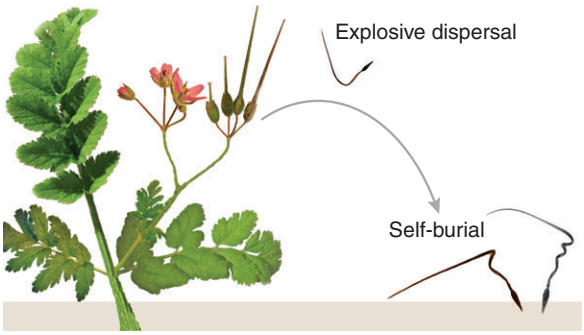

Fig. 1. *Erodium cicutarium* launches seeds up to half a meter using energy stored elastically in a coil-shaped awn that is held straight before dehiscence. The awns subsequently bury the seed by drilling, as they wind and unwind with changes in ambient humidity.

of fracture is the primary measure of success (e.g. Farquhar and Zhao, 2006). Others have applied crack propagation theory to the burrowing of worms in sediment (Dorgan et al., 2005; Dorgan et al., 2007), in which case fracture with the minimum energetic cost is necessary.

Drag could form the basis of another tradeoff (Vogel, 2005; Stamp and Lucas, 1983). For *E. cicutarium* seeds, with elongated, hairy awns, drag is expected to alter the trajectory significantly compared with a zero-drag projectile of the same mass. Drag on seeds reduces the angle of launch at which maximum ballistic range is achieved, flattens the initial trajectory, and reduces the dependence of dispersal distance on initial height (Beer and Swaine, 1977). A seed with lower drag should disperse farther, and drag causes explosively launched seeds to lose between 64 and 94% of their theoretical maximum range in the absence of drag (Vogel, 2005).

However, short-range ballistic launching of a high-drag seed could act to move it to a location with higher wind that may aid dispersal. If the drag on the seed is high enough to reduce its terminal velocity to a value comparable with wind speeds, wind dispersal, which occasionally results in very long dispersal distances, becomes a possibility. It is plausible that disruptive selection between low drag (for high launch distance) or high drag (above some critical value for wind dispersal) could have been relevant in the diversification of the Geraniaceae, which includes species that eject only the low-drag seeds (without attached awns), species that do not eject but instead simply project the carpels outward, and species with intricately branched, hairy, high-drag awns that are primarily wind dispersed (Yeo, 1984; Tokarski, 1972).

Table 1. Awn shape and section properties measured from *E. cicutarium* awns

Parameter	Symbol	Mean ± s.d.
Maximum awn diameter (m)	D	0.002±0.001
Awn height (m)	L	0.015±0.005
Number of turns	n	9±2
Awn spiral angle (deg)	α	86±2 (n=9)
Section width (m)	b	0.001
Section height (m)	h	0.00025
Mass (kg)	m	$5\times10^{-6}\pm1\times10^{-6}$
Terminal velocity (m s^{-1})	v_T	1.6±0.5 (n=24)
Drag coefficient × area (m^2)	C_DA	$3.8\times10^{-5}\pm2\times10^{-5}$ (n=24)

Values are means ± s.d., with measurements from N=34 awns unless otherwise noted. Mean measured values for D, L, n, α, b, h, m and C_DA were used in model computations.

MATERIALS AND METHODS

Erodium cicutarium awns

E. cicutarium (L'Hér) awns were collected over several years (2000–2008) near Merced, Davis and Berkeley, CA, USA. Plants were grown to obtain additional dry awns and fresh green styles. Additional plants and styles were collected in 2007–2009 from roadsides in Marin and Berkeley. Morphological data from 34 *E. cicutarium* awns are given in Table 1.

Movements and shape change during self-burial

Self-burial of individual awns was filmed using time-lapse video (DCR-HC42, Sony Corp., Tokyo, Japan; D80, Nikon Corp., Tokyo, Japan) at frame rates between 0.25 and 1 frame s^{-1}. Awns were filmed on sandy soil and on paper towels after soaking with water from a spray bottle. Awns were also held in a vertical position using polymer clay (Polyform Products Co., Elk Grove Village, IL, USA). To quantify awn motions, awns were filmed from the side and from above. Seed and awn tip positions were digitized using GraphClick (Arizona Software, Neuchâtel, Switzerland). These recordings were then compared with predictions from a model.

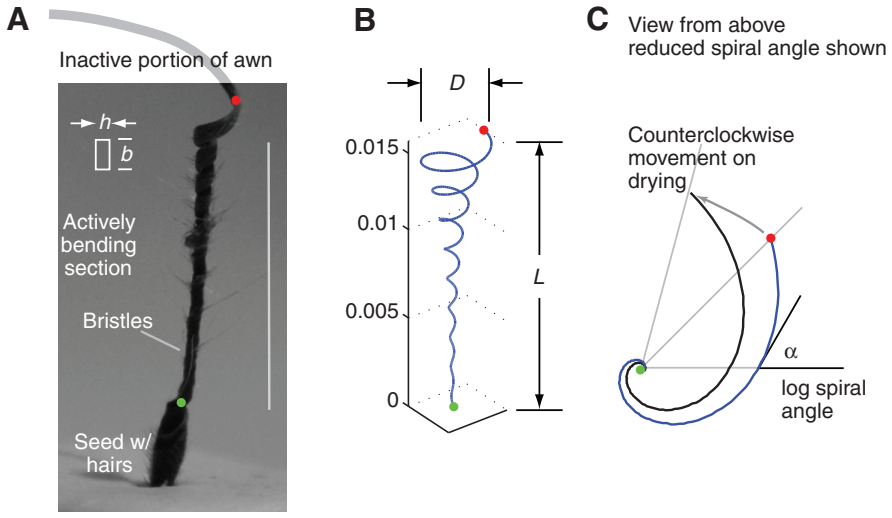

Fig. 2. *E. cicutarium* awn. (A) photograph and (B,C) model. The hygroscopically active portion is the helical middle, and the slightly curved inactive portion is shown 'in phantom'. Model shape parameters are the maximum diameter D, height L, number of turns n, spiral angle α and section width b and thickness h. Digitized landmarks for data plotted in Figs 3–5 and 8 are shown by colored dots: the proximal (seed) end of the active region is shown in green and the distal end of the active region is shown in red. Scale bar, 15 mm.

Table 2. Awn material and section properties assumed in modeling

Parameter	Symbol	Simulation value
Young's modulus (Pa)	E	9×10^{9}
Poisson's ratio	ν	0.33
Shear modulus (Pa)	G	3.4×10^{9}
Work of fracture (J m^{-2})	G_c	150
Second moment of area (m^4)	I	1.3×10^{-15}
Flexural stiffness (N m^2)	EI	1.2×10^{-5}
Initial style height (m)	h_0	0.10
Energy lost in stem recoil	δ_{recoil}	25%
Energy lost in rotation	$\delta_{rotation}$	30%

Material properties based on properties for wood, parallel to the grain (Ashby and Jones, 1996; Vogel, 2003).
Energy lost in stem recoil was estimated assuming the mass of the remaining fruit and stem are large compared with the ejected awn; energy lost in rotation estimated from observed launch speed and rates of rotation (Table 3).

A finite element model (Fig. 2) of the active region of the *Erodium* awn was used to compute shape changes with desiccation during burial. The model, implemented in Matlab (The MathWorks, Natick, MA, USA), included bending terms for a beam of rectangular cross section (Craig, 2000). The cross-sectional geometry was ascertained using hand sections, and the material properties were selected from values reported for wood (Ashby and Jones, 1996; Vogel, 2003; Beer et al., 2005) and wheat awns, which exhibit a similar self-burial behavior (Elbaum et al., 2007) (Table 2). The finite element model was validated by comparing the predicted awn geometry with that observed with the time-lapse video.

Awn shape was specified by the curvature and torsion of the awn axis (Kreysig, 1999; Crenshaw, 2000). This formulation was used because curvature is also used to compute bending moments in beam theory. The curvature and torsion terms may be thought of as 'pitch' and 'roll' for a trajectory along the neutral axis of the awn. Together with the arc length along the awn, any three-dimensional beam structure can be described; the method used here could be applied to other awns or to the movement of tendrils, vines or pollen tubes.

To derive curvature and torsion, the initial awn shape (r) was modeled as a logarithmic spiral ($r=ae^{m\theta}$) stretched in the z direction to form a gradually opening helix. The shape is defined parametrically as a function of a dummy variable, t=[0,1], used for shape calculations:

$$r(t) = D / 2\, e^{\cot(\alpha)\theta}, \tag{1}$$

$$\theta(t) = 2\,\pi n\,(t-1), \tag{2}$$

$$z(t) = Lt. \tag{3}$$

Awn shape was completely defined by four parameters: maximum awn diameter, D; spiral angle, α; number of turns, n; and awn height, L. These parameters were determined from dry *E. cicutarium* awn specimens, as given in Table 1. The parametric description of awn shape in Eqns 1–3 was then converted to one using arc length, curvature and torsion. Arc length, defined along the length of the awn from the seed (t=0) to the distal tip (t=1), was obtained through integration:

$$s(t) = \int_0^t \sqrt{\mathbf{r}'\cdot\mathbf{r}'}\,\mathrm{d}\xi, \tag{4}$$

where $\mathbf{r}=[r(t),\theta(t),z(t)]$ is the position vector from Eqns 1–3 and $\mathbf{r}'$ is the first derivative, $\mathrm{d}\mathbf{r}/\mathrm{d}t$. Computation of torsion and curvature requires tangential vectors pointing along the curved axis of the awn. These were obtained numerically using normalized two-point forward differences:

$$\mathbf{u}(s) = \mathbf{r}'(s), \tag{5}$$

where $\mathbf{u}$ is the tangential vector of the awn finite element.

Further use of two-point forward differences provided the curvature, $\kappa(s)$, unit principal normal vector, $\mathbf{p}$, unit binormal vector, $\mathbf{b}$, and torsion, $\tau(s)$, after Kreysig and Crenshaw (Kreysig, 1999; Crenshaw, 2000):

$$\kappa(s) = |\mathbf{u}'(s)| = |\mathbf{r}''(s)|, \tag{6}$$

$$\mathbf{p} = \frac{1}{|\mathbf{u}'|}\mathbf{u}' = \frac{1}{\kappa}\mathbf{u}', \tag{7}$$

$$\mathbf{b} = \mathbf{u}\mathbf{p}, \tag{8}$$

$$\tau(s) = -\mathbf{p}(s)\cdot\mathbf{b}'(s). \tag{9}$$

Eqns 6–9 are sufficient to define a curve in three-dimensional space (Kreysig, 1999; Crenshaw, 2000). To make them easier to solve computationally, the equations were rearranged into a form called the Frenet equations (Eqn 10) (Kreysig, 1999; Crenshaw, 2000), which was then cast into first-order canonical form and integrated using a fourth-order Runge–Kutta method:

$$\begin{aligned} \mathbf{u}' &= \kappa\mathbf{p} \\ \mathbf{p}' &= -\kappa\mathbf{u} + \tau\mathbf{b} \\ \mathbf{b}' &= -\tau\mathbf{p} \end{aligned}. \tag{10}$$

The curvature changes as variations in humidity create internal bending moments. To simulate hydration and desiccation, a desiccation factor x_d=[0,1] was used as a premultiplier for the curvature estimates from the dry shape, and the Frenet equations were re-integrated to determine the new shape of the awn. This approach provided simulations from complete desiccation (x_d=1) to total hydration (x_d=0). Preliminary environmental scanning electron microscopy (ESEM) work, in which small sections of awns were observed under controlled humidity conditions, showed uniform changes in curvature along the length of the section. This observation suggests that the use of a desiccation factor independent of arc position is valid.

Video recordings of awn movements after wetting were used to validate model predictions of awn shape during wetting and drying. Desiccation (for Fig. 5) was modeled as a first-order time response with a time constant τ_d of 300–400 s. The response is essentially an exponential decay (e^{-t_d/τ_d}) in desiccation during the step change of wetting (from the spray bottle) and an exponential rise (possibly with a different time constant) in desiccation after the source of wetting was removed. The governing differential equation is:

$$\tau_d\frac{\mathrm{d}x_d}{\mathrm{d}t_d} = -x_d + \bar{w}, \tag{11}$$

where $\bar{w}$ (applied wetting) is 0 when the awn is wet (visible in videos from the glistening of the moist surfaces) and 1 when the excess water is no longer visible. The awn is initially fully dry [$x_d(0)$=1].

Energy storage, fracture mechanics and energy at launch

The amount of energy stored in the awn before launch was estimated using Castigliano's theorem (Craig, 2000):

$$U_{elastic} = \frac{1}{2}\int_0^s \frac{M^2}{EI}\,\mathrm{d}s, \tag{12}$$

Table 3. Kinematic data from high-speed video of *E. cicutarium* launches and predicted values from the model using parameters from Tables 1 and 2

Parameter	Observed (mean ± s.d.*)	Predicted
Initial launch speed ($m\,s^{-1}$)	4±2	5.1
Initial angular velocity ($rad\,s^{-1}$)	200±100	182
Launch angle (deg)	40±30	set to 40
Desiccation at launch (estimated from shape)	0.1±0.05	set to 0.1
Distance thrown (m)	0.51±0.08	0.50

*Means of eight launches.

where M is bending moment, E is Young's modulus, I is the second moment of area and the integral is taken over the entire length of the awn. To obtain bending moments, the moment–curvature relationship is used with the curvature estimates obtained from the finite element above (Eqn 10) (Craig, 2000):

$$M = EI\kappa\,, \tag{13}$$

where $I=bh^3/12$ for a rectangular cross section and EI is the flexural stiffness of the beam.

The awn is released when the zone of contact between it and adjacent awns fractures. Energy release during launch was estimated using the fracture mechanics of a propagating crack (reviewed by Vogel, 2003; Craig, 2000; Farquhar and Zhao, 2006; Dorgan et al., 2005; Dorgan et al., 2007). As the cracks between the launching awn and those adjacent to it grow, the energy stored elastically ($U_{elastic}$; calculated above from Eqn 12) is released and used to grow the cracks further:

$$\Delta U = U_{elastic}(x) - U_{surf}(x)\,, \tag{14}$$

where $U_{elastic}(x)$ here is the same integral as Eqn 12 with the upper limit replaced by x. $U_{elastic}(x)$ represents the portion of the elastic energy that is released when a crack of length x frees that portion of the awn from the style and prevents it from developing bending moments. The surface energy required to grow the crack, $U_{surf}(x)$ (energy that is lost during fracture) was estimated from the work of fracture (Farquhar and Zhao, 2006; Vogel, 2003):

$$U_{surf}(x) = 2G_c\,h\,x\,, \tag{15}$$

where G_c is the work of fracture (in $J\,m^{-2}$). We used $G_c=150\,J\,m^{-2}$ based on tabulated values for wood parallel to the grain (Vogel, 2003); we also evaluated the effect of changes in G_c, described below. The crack will propagate to completion, releasing the awn, when the crack length has grown to a critical size where the rate of elastic energy release exceeds the energy required to form new surface, i.e. when $d\Delta U/dx>0$. This point was found numerically from the finite element model bending moments using a Newton–Raphson method.

The kinetic energy used in awn translation at launch was then estimated by taking into account energy lost during the fracture process, as well as energy wasted on recoil of the stem and rotation of the seed:

$$U_{launch} = (U_{elastic} - U_{surf})\,(1 - \delta_{recoil})\,(1 - \delta_{rotation})\,, \tag{16}$$

where δ_{recoil} is the fraction of energy lost to recoil of the style and stem and $\delta_{rotation}$ is the fraction of energy lost in rotational modes of the awn, estimated from kinematics. Energy lost in stem recoil (~25%) was estimated assuming the masses of the remaining fruit and stem are large compared with that of the ejected awn. In cases where a single awn was ejected, three or four other awns generally remained; momentum conservation dictates that the energy lost to recoil in this case is 20–25%. Energy lost in rotation (~30%) was estimated on the basis of the observed launch speeds and rates of rotation (Table 3).

Filming of awn launch and modeling of trajectories

Explosive dispersal was filmed using a high-speed video (AOS Technologies AG, Baden-Daettwil, Switzerland) operated at $500\,frame\,s^{-1}$. Ripe awns were cut from potted plants and from wild plants along roadsides in Berkeley, CA, and placed in dry containers for filming. The heat of the lighting was sufficient to dry the awns to the point of launch. Videos were analyzed frame by frame to obtain awn position in flight and initial translational and rotational velocities and launch angle. Immediately after each launch, mass and distance thrown were recorded and a photograph was taken to record shape. The shape at launch was used to estimate the awn desiccation, defined above, by comparing it with the shape of a control awn filmed during the entire desiccation process. Trajectories obtained from high-speed videos and measured dispersal distances were used to validate the fracture mechanics calculations (above) and ballistics calculations (below) by comparison with predicted trajectories and ranges.

The energy remaining after fracture determines the awn initial velocity (U_{launch}), and subsequent movement was determined by ballistic calculations with drag included (Beer and Swaine, 1977; Vogel, 2005), assuming still air. In the x-direction (horizontal), drag was assumed to be the only force acting, whereas in the y-direction (vertical), drag and gravity were assumed. The equations describing ballistics with drag are (Beer and Swaine, 1977; Vogel, 2005):

$$\begin{aligned} \dot{u} &= -\frac{1}{m} C_D A \frac{1}{2} \rho u^2 \\ \dot{v} &= -\boldsymbol{g} - \frac{1}{m} C_D A \frac{1}{2} \rho v |v| \\ \dot{x} &= u \\ \dot{y} &= v \end{aligned}\,, \tag{17}$$

where $\boldsymbol{g}=9.81\,m\,s^{-2}$ is the acceleration of gravity and the square of the vertical velocity is expressed as $v|v|$, so that the changing sign (direction) of the force is accounted for. The Reynolds number at launch ranges between $Re_D=500$ and $Re_L=4000$, and the drag equation given here is appropriate for high Reynolds number. To estimate the drag coefficient, awns were dropped and filmed to determine the terminal velocity (v_T); launch speeds and terminal velocity are similar enough that a constant drag coefficient may be assumed. Un-normalized drag (drag coefficient times area) was determined from the relation $C_DA=2mg/\rho v_T^2$, where m is mass, $\boldsymbol{g}=9.8\,m\,s^{-2}$ is gravitational acceleration and $\rho=1.2\,kg\,m^{-3}$ is the air density.

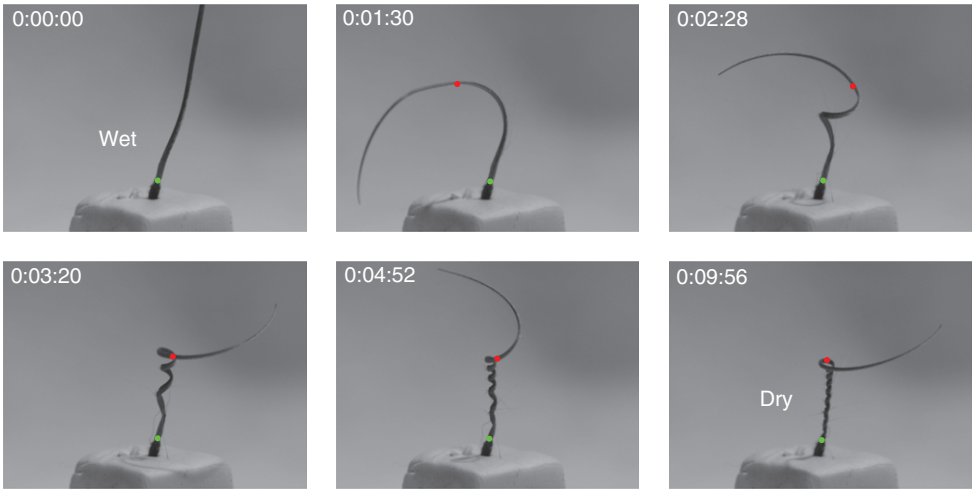

Fig. 3. Representative frames showing awn re-winding upon drying. A soaked awn was placed on polymer clay at time 0:00:00 (h:mm:ss). Green and red dots mark the proximal (seed) and distal ends of the actively bending region. See supplementary material Movie 1.

To solve this set of differential equations requires as initial conditions the initial position and velocity of the awn:

$$\begin{aligned} u(0) &= \sqrt{\frac{2U_{\text{launch}}}{m}}\cos\beta \\ v(0) &= \sqrt{\frac{2U_{\text{launch}}}{m}}\sin\beta \\ x(0) &= 0 \\ y(0) &= h_0 \end{aligned}, \qquad (18)$$

where β is the launch angle and h_0 is the height of the style. The solution, providing the awn launch trajectory and range, was obtained using a fourth-order Runge–Kutta method.

Tradeoffs in the *Erodium* seed launching apparatus

To explore the tradeoffs involved in the *Erodium* seed launching apparatus, we examined the sensitivity of the model related to fracture (material properties E and G_c) and to drag (C_DA). Additionally, because the potential for long-term environmental variation such as warming to alter timing or effectiveness of dispersal, we examined model sensitivity to desiccation.

For each set of model parameters, the finite element model was used to calculate the energy storage as a function of desiccation; the energies were then used to compute dispersal distances using the fracture and ballistic equations. For each comparison, parameters were varied (50, 90, 100, 110 and 150% for E; 50, 66, 100 and 150% for G_c; and 200% for C_DA) one at a time to determine the effect on energy at launch, distance thrown and critical crack length. The effect of varying geometrical parameters (L, D and m) on dispersal distance was also computed, but their effects were small in comparison and are not presented in detail here.

RESULTS

Movements and shape change during self-burial

Upon wetting, awns unwound five to ten full turns over the course of ~15 min (supplementary material Movies 1 and 2). On sandy soil, the unwinding movement allowed the seed head to move over the surface occasionally lodging into cracks. After several wetting and drying periods over several days, several seeds became completely buried. These observations confirm descriptions found in the literature (Stamp, 1984).

During the winding process, the awn goes through a series of complex shape changes appearing first to form a large bend before completing one loose coil that slowly tightens as more coils develop toward the seed (Fig. 3, supplementary material Movie 1). This behavior is reproduced with surprising accuracy by our simple model (Fig. 4, supplementary material Movie 3). To quantify the match between the observed awn kinematics and the model, we recorded the radial distance from the awn axis to the distal end of the active

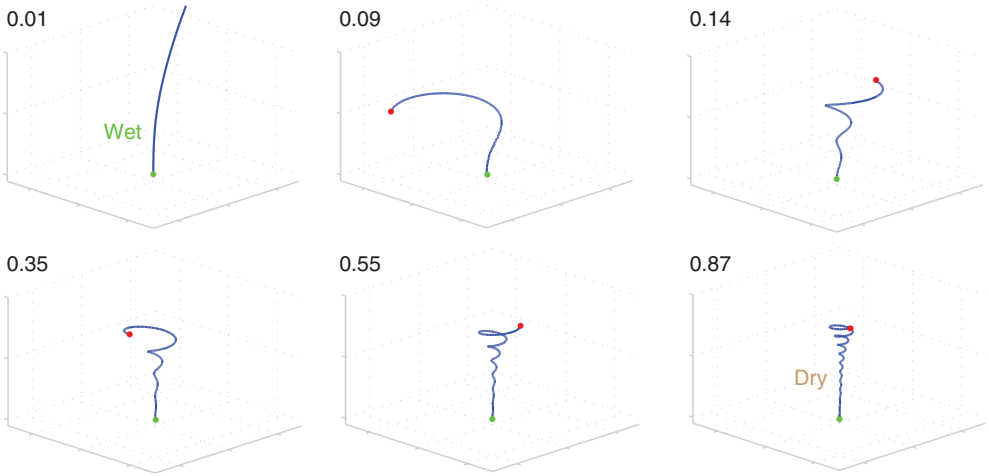

Fig. 4. Model predictions for shape of actively bending region of *E. cicutarium* awns during drying. The predicted shapes correspond well with the observed shapes (Fig. 3). Desiccation factors (x_d) for each shape are noted in the top left corner. Green and red dots represent proximal and distal ends of actively bending region, as in Fig. 3. See supplementary material Movie 3.

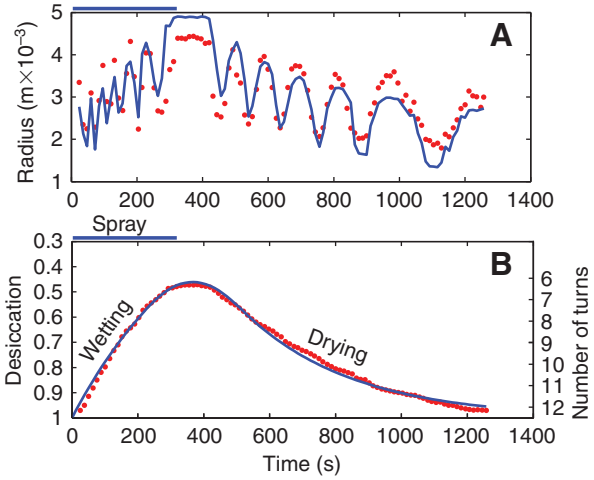

Fig. 5. (A) Radial distance of distal end of active region (red dot in Fig. 2) from central axis as a function of time during a wetting and drying transient. Measured positions are shown in red, model predictions, in blue. Wetting period shown with blue overline. (B) Number of turns and desiccation as a function of time for wetting and drying transient. Measured number of turns is shown in red: the blue line indicates a simple first order step response to the wetting with the time constant (τ_d)=330 s on wetting and τ_d=400 s on drying (Eqn 11).

region during partial wetting and drying (Fig. 5), as viewed from above. We find that by varying a single parameter, the desiccation factor (x_d), we can reproduce the intricate motion of the awn in precise quantitative terms. We also find that the wetting dynamics can be approximated by a first order decay with 330 s time constant on wetting and 400 s time constant on drying. Having established that the model captures accurately the kinematics of the awn, we used it to explore its mechanical aspects, in particular the storage of elastic energy that powers the explosive dispersal.

Energy storage and fracture mechanics at launch

Based on the geometry of awns right after launch, we determined that a desiccation factor of approximately 10% is achieved before explosive fracture. Using this information, we were able to map the curvature and bending moments (from Eqn 10) present along the length of the awn (Fig. 6). Integrating the local bending energy (Eqn 12) reveals how much elastic energy is freed by a propagating crack (Fig. 7A). Some of this energy is used to create new surfaces (Eqn 15), and the difference between these two energies is the net energy released. The critical crack length, at which the crack will propagate and the awn should launch, occurs where the slope of the net energy *versus* crack length curve switches sign. We predict a critical crack length of approximately 3 mm (Fig. 7). We were not able to directly measure the critical crack length, however, this distance is a reasonable estimate on the based on the position of the seed before launch and from awns mechanically forced to launch using a dissecting probe. Predictions for energy at launch and initial launch speeds are given in Tables 3 and 4.

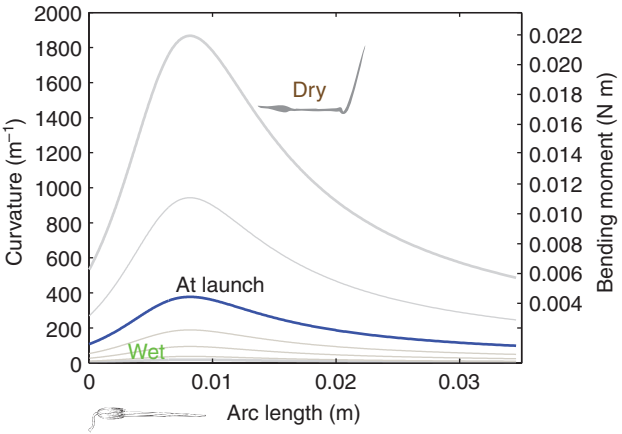

Fig. 6. Curvature and bending moment in model awn as a function of arc length and desiccation. The blue line shows the curvature and bending moment at 10% desiccation (x_d=0.1), typical of awns at launch. Bending moments are concentrated in the proximal half of the awn.

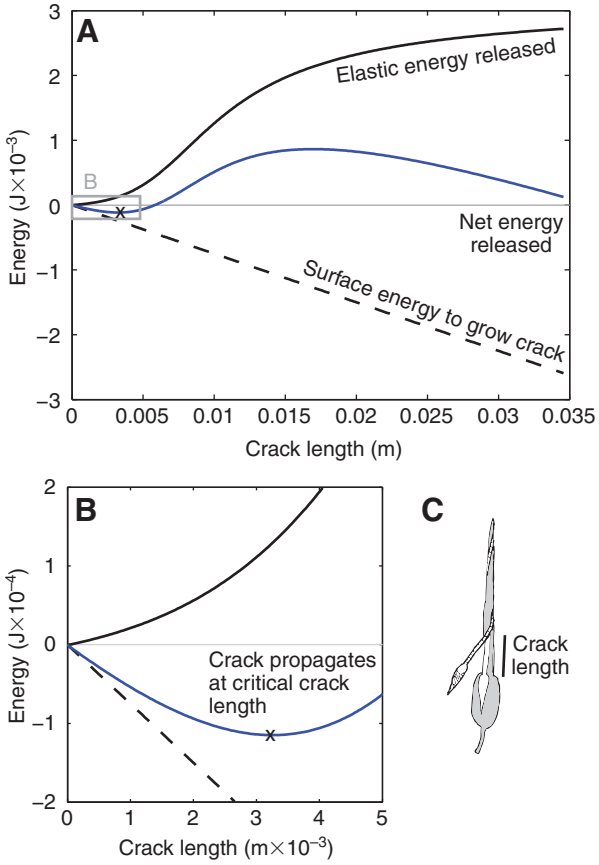

Fig. 7. (A) Fracture mechanics of *E. cicutarium* awn launch, according to the energy storage model at 10% desiccation (x_d=0.10). The dotted line indicates the energy required to form a new surface as the awn breaks away. The solid line indicates elastic energy released as the awn breaks away from seed to tip. The blue line indicates the net energy released. (B) Fracture occurs at crack lengths greater than the critical crack length (indicated by x) where the slope of the net energy released becomes positive. Momentum of the seed will also continue to grow the crack. Crack length is taken to be arc length (C). Energy storage is concentrated in the proximal half of the style.

Filming of awn launch and modeling of trajectories

Eight launches were captured on high-speed video (summary in Table 3, example trajectory in Fig. 8; supplementary material Movies 4 and 5). Upon release, ripe *E. cicutarium* awns were thrown at an

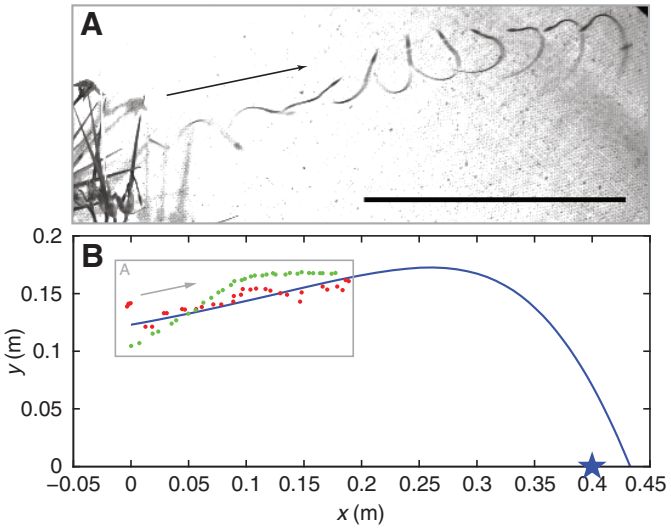

Fig. 8. (A) Representative initial launch trajectory, shown by multiple exposures at 4 ms intervals. Movement is from left to right. (B) Predicted trajectory with drag matches the initial launch trajectory [inset box, seed (green) and tip (red) positions shown at 2 ms intervals] and final distance thrown (blue star). Scale bar, 10 cm. See supplementary material Movie 4.

angle of 40±30 deg (mean ± s.d., n=8) and covered a distance of 0.51±0.08 m. Filming of the launch showed average initial translational and rotational velocities of 4±2 m s^{-1} and 200±100 rad s^{-1}, respectively. The observed trajectories compare well with computed trajectories based on the measured initial launch parameters [$u(0)$, $v(0)$, h_0] and drag coefficient (Fig. 8B). Predictions for launch speeds and dispersal distance fell within measured values (Tables 3 and 4). Trajectories had fairly high initial velocities with straight initial sections and short ranges (considering the initial velocity), which is a characteristic of high drag, as expected from other work on the launch of spores and seeds (Vogel, 2005; Beer and Swaine, 1977; Noblin et al., 2009).

Tradeoffs in the *Erodium* seed launching apparatus

Tradeoffs involved in the *Erodium* seed launching apparatus are shown in Fig. 9. Variation in E (50, 90, 100, 110 and 150%) is shown in Fig. 9A; variation in G_c (50, 66, 100, 150 and 200%) in Fig. 9B and D; and variation in C_DA (50, 66, 100, 150 and 200%) in Fig. 9C. *Erodium* launches appear to be near a 'knee' in curves for dispersal distance. Drag and fracture mechanics have the potential to greatly alter dispersal distance, and the significance of these is discussed below.

DISCUSSION

The beam bending equations (Eqns 1–10) predict the shape changes of *E. cicutarium* awns during hygroscopic movement, as shown by the overall shapes in Figs 3 and 4 and the motion of the distal end of the active region (Fig. 5). The energy and ballistic equations (Eqns 12–18) predict trajectories (Fig. 8) and dispersal distances similar to those observed here (measured distance: 0.51±0.08 m; predicted distance: 0.58 m) and by Stamp (Stamp, 1989a), who found seeds of *Erodium moschatum* were flung an average of 0.56 m.

The time response to wetting (Eqn 11, Fig. 5) is consistent with a first order response with a time constant of 330 s on wetting or 400 s on drying. Further work is needed to look at the cellular basis for the hygroscopic behavior of the tissue. In addition, the profiles of bending moment, which set the awn shape, develop in the growing awn through some sort of axial patterning that establishes regions of bending in the middle to distal region and regions of torsion in the proximal to middle region. Finally, the model sensitivity calculations described below bound the effects of variation in material properties such as the Young's modulus and fracture toughness, and further histological studies could connect such macroscopic properties to tissue structure.

Energetics of seed launching in *Erodium* compared with others

Seed launching in *E. cicutarium* is costly compared with similarly sized jumping animals. Approximately 0.003 J is stored in a ripe awn held in a straight configuration (Table 4). Only 0.3% of the

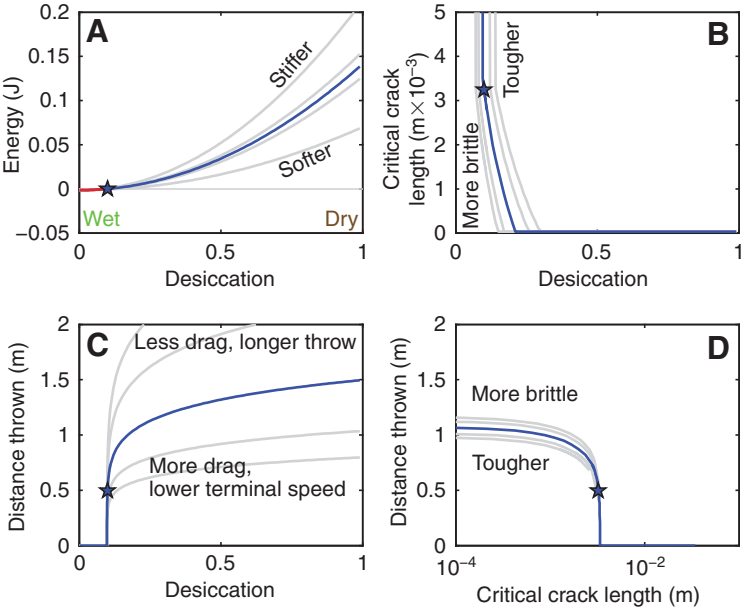

Fig. 9. Model sensitivity and tradeoffs between dispersal distance (range) and avoidance of 'duds' (critical crack size), according to the energy storage model. Stars indicate the average desiccation observed in newly launched awns. (A) Awns that are too wet do not store enough energy to fling (red portion on left); the higher the desiccation, the higher the energy storage and the greater the dispersal distance. (B) Overly wet duds are avoided by long critical crack sizes (upper left). However, this limits the maximum desiccation attainable with short critical crack sizes at higher stresses (lower right). (C,D) *E. cicutarium* appears to compromise by breaking at a point of diminishing return in range. A tougher trigger could allow higher stored elastic energy but would also reduce the launch energy by increasing the surface energy and increasing the risk of duds. (C) Under favorable conditions, *Erodium* might be expected to reach 1 m range. Reductions in drag coefficient could double the range or more, whereas increases could reduce the terminal velocity to speeds comparable with wind speeds.

Table 4. Energy budget for *E. cicutarium* launch simulation

Elastic energy released (J)	2718×10^{-6}
Surface energy lost during break (J)	-2592×10^{-6}
25% energy lost to recoil of stem (J)	-32×10^{-6}
30% energy lost in rotational modes of awn (J)	-28×10^{-6}
Energy remaining in seed translation	66×10^{-6}
Distance thrown, without drag (m)	2.7
Distance thrown, with drag (m)	0.50
Percentage of range lost to drag	81%

initial stored energy is imparted to awn translation. The mechanical cost of transport is $26\,J\,kg^{-1}\,m^{-1}$, whereas the elastic energy storage required is $\sim1000\,J\,kg^{-1}\,m^{-1}$. These reflect loss of transmission of elastically stored energy and the effect of drag; the estimated range without drag is 2.7 m (Table 4). These results are similar to other spring-launched seeds; in *Impatiens capensis*, 0.5% of stored elastic energy is transferred to seed movement and the overall cost of transport is $280\,J\,kg^{-1}\,m^{-1}$ (Hayashi et al., 2009). Animals, however, tend to be more economical. In many hexapedal runners, the mechanical cost of transport is approximately $1\,J\,kg^{-1}\,m^{-1}$ (Full, 2001), $4.9\,J\,kg^{-1}\,m^{-1}$ for an ideal ballistic jumper without drag, or $\sim6\,J\,kg^{-1}\,m^{-1}$ for a 5 mg amphipod (D.E., M. Perry and C. Ng, in preparation).

The high cost for seed launching in *E. cicutarium* reflects how dispersal is a slightly different problem from jumping in animals. First, seed launch is a one-time jump closely linked to fitness in an organism, with fewer alternative means of transportation than mobile animals. Second, in common with other small jumpers, drag plays a proportionately larger role in determining range, and nondimensional metrics are available to gauge its effect (Vogel, 2005). For *E. cicutarium*, 81% of the theoretical range in a vacuum is lost to drag. A nondimensional index of the degree to which drag alters the ballistic trajectory can also be calculated by balancing gravitational and fluid forces [(Vogel, 2005) modified here based on mass; m]:

$$RI = 2110\left[\frac{m^2}{v_o^3 Lbh}\right]^{0.5}, \qquad (19)$$

where L, b and h are as previously defined and v_o is the initial velocity (magnitude of first two terms of Eqn 18). A projectile with a range index (RI)>100 is relatively unaffected by drag, whereas one with a low RI should have a much shorter range. For *E. cicutarium*, RI is approximately 11. Compared with ballistic seeds, *E. cicutarium* is in the middle of the range of speeds, dispersal distance lost to drag and RI. Seed dispersal of the tropical tree *Hura crepitans* (RI=2, 90% of range lost to drag) is much faster than that of *E. cicutarium* at $70\,m\,s^{-1}$, and loses a higher percentage of its range to drag at this extreme speed. However, other ballistic seeds with similar RI, such as those of hogwort (*Croton capitatus*; 37% of range lost to drag), vetch (*Vicia sativa*; 49.9% of range lost to drag) or the petunia (*Ruellia brittoniana*; 66.5% of range lost to drag), lose less of their range to drag than *Erodium* (Vogel, 2005). At slower speeds, *Impatiens capensis* seeds achieve velocities of $1.24\,m\,s^{-1}$ and lose ~20% of their range to drag (Hayashi et al., 2009). Considering just overall range, seeds of *Euphorbia boetica* travel a median distance of 1.3 m and a maximum of almost 8 m, whereas those of *Euphorbia nicaeensis* travel up to 5 m, both much farther than *Erodium* seeds (Narbona et al., 2005). However, none of these seeds bury themselves, nor do they carry with them the bulk of the launching machinery.

Tradeoffs in the *Erodium* seed launching apparatus

Fig. 9 illustrates some of the tradeoffs between stiffness, toughness, critical crack length, drag and range, and shows that the *Erodium* launches observed here are near a 'knee' in the curves for dispersal distance and critical crack length. Launch angle and height were not considered here, but in other seed-launching plants, such as *V. sativa* and *C. capitatus*, the height of flowers and a slight upward angle of launch appear to provide increases in range relative to random angles and locations low on the plant (Garrison et al., 2000).Fig. 9A shows that awns that are too wet (red line, left side) do not store enough energy to launch, because any cracks in them will not propagate to completion. Fig. 9A also shows the effect of a stiffer or softer material (higher or lower E). Stiffer materials store more energy than softer materials and a 50% increase in E would increase range by up to 60%, except that the critical crack size becomes small, increasing the possibility of a premature launch. A tougher material (higher G_c) may reduce the chance of a premature launch by increasing the critical crack size, as shown in Fig. 9B; however, this will reduce the distance thrown. In contrast, a more brittle awn (lower G_c) will lose less energy while breaking apart during launch, but it will be triggered at lower desiccation than a tougher awn, releasing less energy.

Fig. 9B,D further shows the compromise between fracture mechanics and dispersal distance. Higher energy storage (from higher desiccation) or greater energy release (from a more brittle material) only provides moderately more range, at the risk of more premature launches (a drastically reduced critical crack length). Increased toughness would allow more energy storage or higher desiccation, at the risk of more failed launches and higher energy loss upon launch. Under favorable conditions, such as in a ripe, undisturbed plant allowed to quickly dry all at once, ranges of up to a meter maximum might be expected for *Erodium* (middle blue line, Fig. 9C). To support this prediction, *Erodium moschatum* reached a maximum of 85 cm in dispersal distance experiments in still air (Stamp, 1989a). The interactions between dispersal, desiccation, temperature and humidity could be examined further by combining our mechanistic model with boot-strapped meteorological data (Denny et al., 2006).

Another major determinant of dispersal distance appears to be the drag of the awn (Fig. 9C), with range approximately doubled for a halving of the drag coefficient. This seems reasonable as ranges of up to 3 m are seen in *Geranium maculatum*, *G. carolinianum* and *G. molle* (Stamp and Lucas, 1983), which utilize low-drag seed ejection (Yeo, 1984). However, a doubling of drag coefficient, such as in high-drag carpal projection (Yeo, 1984), would reduce the terminal velocity to below $1\,m\,s^{-1}$, improving chances for wind dispersal. By leaving the launching machinery with the mother plant, the seed ejection range is maximized; however, carpal projection with more branched awns will maximize drag to catch the breeze.

The *Erodium* specimens in this study were collected from windy roadsides and it is probable that both wind and ballistic dispersal are important in *Erodium*. Although we did not examine the effect of wind on *Erodium* launch rates, wind should enhance desiccation, and mechanical forces from wind agitating the style would contribute to crack growth between adjacent awns, both hastening launch. In addition, horizontal and upwards vertical components of wind would increase downwind dispersal distance predicted here.

The mode of seed discharge in *Erodium* appears to have originated early in the evolution of the Geraniaceae (Yeo, 1984; Tokarski, 1972). Transitions from *Erodium*-type discharge, which is ancestral to the Geraniaceae, to seed ejection or carpal projection, seen in

later-evolving relatives of *Erodium* (Yeo, 1984), could be explored further using the models here as part of a comparative study. For such comparative studies, the model developed here could, (1) explicitly evaluate performance effects of trait changes in the seed ejection apparatus, as well as of secondary dispersal models related to self-burial. Further tradeoffs involving the length of the styles, the number of turns and awn diameter could also be examined to explore, (2) the effect on self-burial and hygroscopic movement on the ground, (3) the effect on drag and wind dispersal, and (4) the sensitivity of dispersal to changes in climate, so connecting biomechanics with ecology, phylogeny and evolution.

LIST OF SYMBOLS AND ABBREVIATIONS

A	reference area (m^2)
b	section width (m)
$\mathbf{b}$	unit binormal vector in Frenet equations
C_D	drag coefficient (dimensionless
D	maximum awn diameter (m)
e	base for natural logarithms (2.71828)
E	Young's modulus (Pa)
EI	flexural stiffness (N m^2)
F_D	drag force (N)
G	shear modulus
G_c	work of fracture (J m^{-2})
$\boldsymbol{g}$	gravitational acceleration (9.81 m s^{-2})
h	section height (m)
h_0	initial height (m)
I	second moment of area (m^4)
L	awn height (m)
m	mass (kg)
M	bending moment (N m)
n	number of turns
$\mathbf{p}$	unit principal normal vector in Frenet equations
$\mathbf{r}=(r, \theta, z)$	cylindrical coordinates of awn finite element, radial (m), tangential (rad), and vertical (m), parameterized over awn coordinates [0,1] or arc length s (m)
Re	Reynolds number (dimensionless)
RI	range index (dimensionless)
s	arc length along awn neutral axis (m)
t	position, from proximal to distal, along awn neutral axis [0,1]
t_d	time (s) in desiccation model
$\mathbf{u}$	tangential vector of awn finite element, pointing along neutral axis, in Frenet equations
u	horizontal component of velocity (m s^{-1})
$U_{elastic}$	elastic strain energy (J)
U_{launch}	energy at launch (J)
U_{surf}	surface energy of crack (J)
v	vertical component of velocity (m s^{-1})
v_T	terminal velocity during drop test (m s^{-1})
$\overline{w}$	applied wetting or drying, [0,1], in desiccation model
x_d	dessication factor [0,1]
α	awn spiral angle (rad)
β	launch angle (rad)
δ_{recoil}	fraction of energy lost to recoil during launch, dimensionless
$\delta_{rotation}$	fraction of energy lost to rotation during launch, dimensionless
κ	curvature in Frenet equations (m^{-1})
ν	Poisson's ratio (dimensionless
ξ	dummy variable of integration
ρ	air density (1.2 kg m^{-3})
τ	torsion in Frenet equations (dimensionless)
τ_d	time constant for wetting/drying (s) in desiccation model

ACKNOWLEDGEMENTS

We thank Y. Zeng, M. Koehl, K. Dorgan, Y. Munk and the Koehl Lab, G. Goldsmith, D. Schichnes and S. Ruzin (UC Berkeley) and A. MacDowell (Lawrence Berkeley Labs) for their assistance and comments. High-speed cameras were provided by T. Libby of the Berkeley Center for Integrative Biomechanics in Education and Research (CIBER). Two anonymous reviewers provided useful comments that were incorporated. D.E. was supported by an NSF Minority Graduate Research Fellowship and a UC Berkeley Chancellor's Fellowship.

REFERENCES

Ashby, M. F. and Jones, D. (1996). *Engineering Materials I*, 2nd edition. Oxford: Butterworth-Heinemann.
Baythavong, B., Stanton, M. and Rice, K. (2009). Understanding the consequences of seed dispersal in a heterogenous environment. *Ecology* **90**, 2118-2128.
Beer, P., Sinn, G., Gindl, M. and Tschegg, S. (2005). Work of fracture and chips formation during linear cutting of particle board. *J. Mater. Process. Technol.* **159**, 224-228.
Beer, T. and Swaine, M. D. (1977). On the theory of explosively dispersed seeds. *New Phytol.* **78**, 681-694.
Collins, B. S. and Wein, G. R. (1997). Mass allocation and self-burial of *Aristida tuberculosa* florets. *J. Torrey Bot. Soc.* **124**, 306-311.
Craig, R. J. (2000). *Mechanics of Materials*, 2nd edition. New York: Wiley and Sons.
Crenshaw, H. C. (2000). Analysis of the three-dimensional trajectories of organisms: estimates of velocity, curvature and torsion from positional estimates. *J. Exp. Biol.* **203**, 961-982.
Denny, M. W., Miller, L. and Harley, C. (2006). Thermal stresses on intertidal limpets: long-term hindcasts and lethal limits. *J. Exp. Biol.* **209**, 2420-2431.
Dorgan, K. M., Jumars, P. A., Johnson, B., Boudreau, B. P. and Landis, E. (2005). Burrow extension by crack propagation. *Nature* **433**, 475.
Dorgan, K. M., Arwade, S. R. and Jumars, P. A. (2007). Burrowing in marine muds by crack propagation: kinematics and forces. *J. Exp. Biol.* **210**, 4198-4212.
Elbaum, R., Zaltzman, L., Bugert, I. and Fratzl, P. (2007). The role of wheat awns in the seed dispersal unit. *Science* **316**, 884.
Farquhar, T. and Zhao, Y. (2006). Fracture mechanics and its relevance to botanical structures. *Am. J. Bot.* **93**, 1449-1454.
Full, R. J. (2001). The concepts of efficiency and economy in land locomotion. In *Efficiency and Economy in Animal Physiology* (ed. R. W. Blake). New York: Cambridge University Press.
Garrison, W. J., Miller, G. L. and Raspet, R. (2000). Ballistic seed projection in two herbaceous species. *Am. J. Bot.* **87**, 1257-1264.
Hayashi, M., Feilich, K. L. and Ellerby, D. J. (2009). The mechanics of explosive seed dispersal in orange jewelweed (*Impatiens capensis*). *J. Exp. Bot.* **60**, 2045-2053.
Kreysig, E. J. (1999). *Advanced Engineering Mathematics*, 8th edition. New York: Wiley and Sons.
Mensing, S. and Byrne, R. (1998). Pre-mission invasion of *Erodium cicutarium* in California. *J. Biogeogr.* **25**, 757-762.
Murbach, L. (1900). Note on the mechanics of the seed-burying awns of *Stipa avanacea*. *Bot. Gaz.* **30**, 113-117.
Narbona, E., Arista, M. and Ortiz, P. (2005). Explosive seed dispersal in two perennial Mediterranean *Euphorbia* species (Euphorbiaceae). *Am. J. Bot.* **92**, 510-516.
Noblin, X., Yang, S. and Dumais, J. (2009). Surface tension propulsion of fungal spores. *J. Exp. Biol.* **212**, 2835-2843.
Stamp, N. E. (1984). Self-burial behaviour of *Erodium cicutarium* seeds. *J. Ecol.* **72**, 611-620.
Stamp, N. E. (1989a). Efficacy of explosive versus hygroscopic seed dispersal by an annual grassland species. *Am. J. Bot.* **76**, 555-561.
Stamp, N. E. (1989b). Seed dispersal of four sympatric grassland annual species of *Erodium*. *J. Ecol.* **77**, 1005-1020.
Stamp, N. E. and Lucas, J. R. (1983). Ecological correlates of explosive seed dispersal. *Oecologia* **59**, 272-278.
Tokarski, M. (1972). Morphological and taxonomical analysis of fruits and seeds of the European and Caucasian species of the genus *Geranium*. *Monographiae Botanicae, Polskie Towarzystwo Botaniczne* **36**, 5-115.
Vogel, S. (2003). *Comparative Biomechanics: Life's Physical World.* Princeton, NJ: Princeton University Press.
Vogel, S. (2005). Living in a physical world. II. The bio-ballistics of small projectiles. *J. Biosci.* **30**, 167-175.
Wolgemuth, C. (2009). Plant biomechanics: using shape to steal motion. *Curr. Biol.* **19**, 409-410.
Yeo, P. F. (1984). Fruit discharge type in *Geranium* (Geraniaceae): its use in classification and its evolutionary implications. *Bot. J. Linn. Soc.* **89**, 1-36.